Computers in Biology and Medicine 102 (2018) 30–39

Contents lists available at ScienceDirect

Computers in Biology and Medicine

journal homepage: www.elsevier.com/locate/compbiomed

Predicting conversion from MCI to AD by integrating rs-fMRI and structural MRI

Seyed Hani Hojjati[a], Ata Ebrahimzadeh[a], Ali Khazaee[b], Abbas Babajani-Feremi[c,d,e,*], for the Alzheimer's Disease Neuroimaging Initiative[1]

[a] Department of Electrical Engineering, Babol University of Technology, Babol, Iran
[b] Department of Electrical Engineering, University of Bojnord, Bojnord, Iran
[c] Department of Pediatrics, University of Tennessee Health Science Center, Memphis, TN, USA
[d] Department of Anatomy and Neurobiology, University of Tennessee Health Science Center, Memphis, TN, USA
[e] Neuroscience Institute and Children's Foundation Research Institute, Le Bonheur Children's Hospital, Memphis, TN, USA

ARTICLE INFO

Keywords:
Alzheimer's disease (AD)
Mild cognitive impairment (MCI)
Structural MRI
Resting-state fMRI
Graph theory
Machine learning approach

ABSTRACT

Structural MRI (sMRI) and resting-state functional MRI (rs-fMRI) have provided promising results in the diagnosis of Alzheimer's disease (AD), though the utility of integrating sMRI with rs-fMRI has not been explored thoroughly. We investigated the performances of rs-fMRI and sMRI in single modality and multi-modality approaches for classifying patients with mild cognitive impairment (MCI) who progress to probable AD-MCI converter (MCI-C) from those with MCI who do not progress to probable AD-MCI non-converter (MCI-NC). The cortical and subcortical measurements, e.g. cortical thickness, extracted from sMRI and graph measures extracted from rs-fMRI functional connectivity were used as features in our algorithm. We trained and tested a support vector machine to classify MCI-C from MCI-NC using rs-fMRI and sMRI features. Our algorithm for classifying MCI-C and MCI-NC utilized a small number of optimal features and achieved accuracies of 89% for sMRI, 93% for rs-fMRI, and 97% for the combination of sMRI with rs-fMRI. To our knowledge, this is the first study that investigated integration of rs-fMRI and sMRI for identification of the early stage of AD. Our findings shed light on integration of sMRI with rs-fMRI for identification of the early stages of AD.

1. Introduction

Alzheimer's disease (AD), a progressive, irreversible neurodegenerative disorder, occurs most frequently in older adults and gradually destroys regions of the brain that are responsible for memory, thinking, learning, and behavior. The diagnoses of AD and its prodromal stage referred to as mild cognitive impairment (MCI) have attracted much attention in recent decades. MCI refers to a clinical syndrome characterized by significant cognitive impairments, which are beyond normal for healthy adults, but not sufficient to meet clinical criteria for AD. The rate of conversion from MCI to overt dementia is substantial, at 15% per year [1]. The amnestic subtype of MCI has a high risk of progression to AD, constituting a prodromal stage of AD [2].

Biomarkers based on positron emission tomography (PET), structural magnetic resonance imaging (sMRI), and resting-state functional MRI (rs-fMRI) have provided promising results for discriminating MCI from AD [3–5]. MRI-based biomarkers have been used to identify the early stage of AD [6–8]. In a recent study, six anatomical MRI measures, e.g. cortical surface area and subcortical volumes, were used to discriminate AD patients from controls, and an area under the receiver operating characteristic (ROC) curve (AUC) of 0.98 was reported [9]. Eskildsen et al. [6] used patterns of cortical thickness and identified cortical regions potentially discriminative for separating MCI converter (MCI-C) patients from MCI patients who remained stable for three years (MCI-NC). They reported a maximum accuracy of 76% for classifying MCI-C from MCI-NC.

The rs-fMRI connectivity analysis can assist in the diagnosis of diseases associated with alteration of the brain network, even before

* Corresponding author. Department of Pediatrics, University of Tennessee Health Science Center, Neuroscience Institute, Le Bonheur Children's Hospital, 848 Adams Ave, Suite L445A, Memphis, TN 38105, USA.
E-mail address: ababajan@uthsc.edu (A. Babajani-Feremi).

[1] Data used in preparation of this article were obtained from the Alzheimer's Disease Neuroimaging Initiative (ADNI) database (adni.loni.usc.edu). As such, the investigators within the ADNI contributed to the design and implementation of ADNI and/or provided data but did not participate in analysis or writing of this report. A complete listing of ADNI investigators can be found at: http://adni.loni.usc.edu/wp-content/uploads/how_to_apply/ADNI_Acknowledgement_List.pdf.

https://doi.org/10.1016/j.compbiomed.2018.09.004
Received 18 June 2018; Received in revised form 6 September 2018; Accepted 9 September 2018

brain atrophy has emerged. Since cognitive and behavioral functions rely on large-scale network interactions, the rs-fMRI connectivity analysis may clarify fundamental aspects of disease pathophysiology [10]. The rs-fMRI connectivity analysis has been utilized to detect alteration of the brain networks in MCI and AD [11–15]. A previous study reported that some brain networks were selectively disrupted in AD, while other networks might be affected by AD pathology at the early stage of AD [16]. While previous studies demonstrated the ability of rs-fMRI in the identification of patients with AD from healthy controls or patients with MCI [17–21], the utility of rs-fMRI in the prediction of the early stage of AD, also the classification of MCI-C from MCI-NC, has not been completely explored [22].

AD has been associated with several imaging biomarkers, including brain atrophy measured through sMRI, particularly in the hippocampus and posterior cingulate gyrus [23,24], hypometabolism in the temporal and parietal lobes measured via FDG-PET [25,26], and abnormal fractional anisotropy (FA) and mean diffusivity (MD) in hippocampus and other structures [27–29]. It is expected that the biomarkers based on these neuroimaging modalities have complementary information, and thus a multi-modal approach may improve our understanding of AD over that presented by one modality [28]. Previous neuroimaging studies in the diagnosis of AD have mainly focused on single modality approaches, although some evidence has demonstrated that a multi-modal imaging approach can improve accuracy of this diagnosis [5]. Previous multi-modal studies in AD diagnosis have integrated MRI, diffusion tensor imaging (DTI), PET, cerebral blood flow (CBF), and/or electroencephalography (EEG) [30,31]. Arbabshirani et al. [32] performed a comprehensive review of neuroimaging-based single subject prediction for MCI, AD, and other neurological and psychiatric diseases. They concluded that: 1) there is widespread evidence demonstrating the potential of neuroimaging data for prediction of AD and other diseases; and 2) most studies reported superior performance of a multi-modal approach compared to single modality. Hinrichs et al. [33] reported that clinical and imaging data (MRI and fludeoxyglucose (FDG)-PET) can be successfully combined to predict AD using machine-learning techniques. They found that the imaging modalities had a better performance in prediction of AD compared to clinical data [33]. The complementary aspects of EEG and sMRI data in the modeling of language ability and other cognitive functions in pathologic aging have been demonstrated [34,35]. It was reported that patients with MCI can be identified using a combination of the amplitude of the resting-state EEG in alpha band and the hippocampal atrophy, extracted from sMRI [36,37].

Previous studies integrated rs-fMRI with other imaging modalities in AD diagnosis, although the results of these studies are not consistent [38,39]. Some of these studies reported that integrating rs-fMRI with other modalities improved the performance of classifying AD from controls [39,40]. It was also reported that this integration did not improve performance of the classification [38]. Schouten et al. [39] investigated the performances of uni-modal and multi-modal approaches for classification of patients with MCI and AD using an elastic net classifier based on several measures derived from sMRI, DTI, and rs-fMRI. They reported that the AUC of unimodal classification ranged from 0.76 for rs-fMRI to 0.91 for sMRI. They obtained an AUC of 0.95 for the classification of patients with MCI and AD by combining sMRI, DWI, and rs-fMRI measures. They concluded that combining multiple MRI modalities can considerably improve classification performance over uni-modal classification. Dyrba et al. [38] investigated a multi-modal approach based on sMRI, DTI, and rs-fMRI to classify AD from HC using support vector machine (SVM). They obtain an AUC of 86% for sMRI, 87% for DTI, and 80% for rs-fMRI to classify AD from HC using a single modality approach. For multi-modal approaches, they obtained an AUC of 82% using all three modalities and 89% using a combination of DTI with sMRI. They concluded that combining rs-fMRI with other MRI modalities may not significantly improve classification accuracy compared to SMRI or DTI alone.

In addition to the discrepancy in the literature about whether or not integration of rs-fMRI with other imaging modalities can improve accuracy of AD classification, there is no study to evaluate the performance of integrating rs-fMRI with other modalities, e.g., sMRI, in prediction of the early stage of AD and classifying MCI-C from MCI-NC. To address these deficiencies, we evaluated the performances of rs-fMRI and sMRI in single modality and multi-modality approaches to predict the early stage of AD. To achieve the best performance in this prediction, we investigated the application of two atlases for parcellation of the brain regions for each modality. After extraction of graph measures from rs-fMRI and structural measures, e.g., cortical thickness, from sMRI, we used these measures as input features of our feature selection algorithm to identify a small subset of optimal features. Selection of appropriate features not only removes the non-informative inputs, but it also reduces the computational time involved in classification [41]. We utilized these optimal features in a machine learning approach based on the SVM to accurately classify MCI-C from MCI-NC.

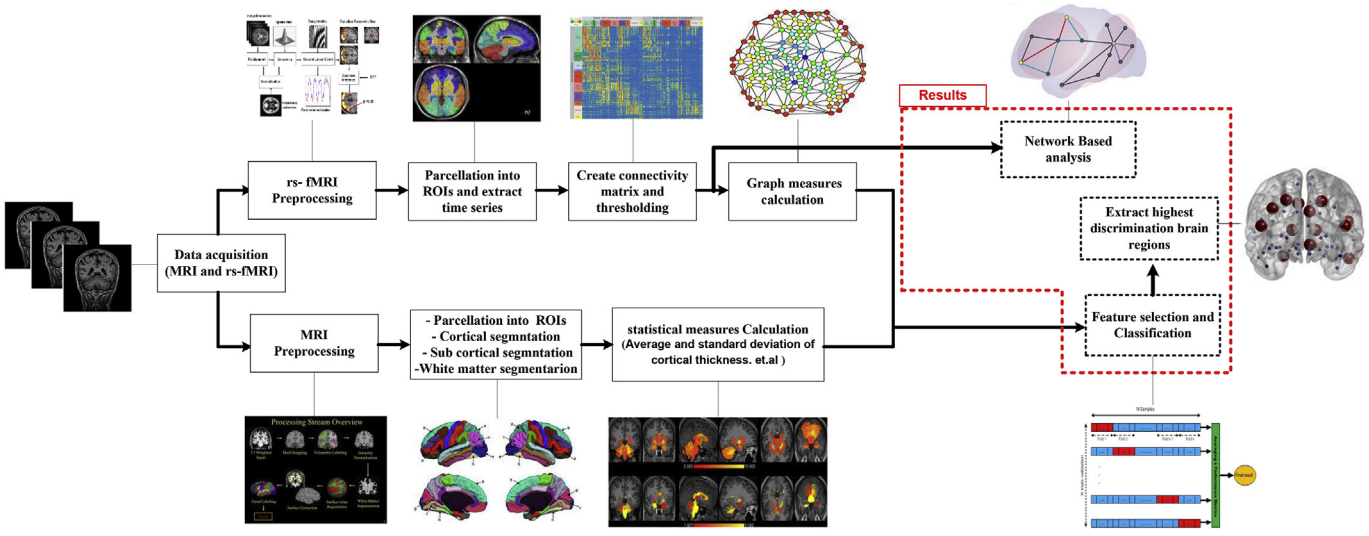

Fig. 1. The overall procedure for this study.

2. Methods

2.1. Overall procedure

The overall procedure of this study is shown in Fig. 1. After preprocessing of rs-fMRI data, we employed the automated anatomical labeling (AAL) atlas [42] and the Dosenbach atlas [43] for parcellation. The rs-fMRI time series of 90 and 160 region of interests (ROIs) in the AAL and Dosenbach atlas were extracted to calculate two connectivity matrices for each of 18 MCI-C and 62 MCI-NC subjects (Table 1). The connectivity matrices were then thresholded to compute 10 local and 13 global graph measures. For sMRI images, we utilized the FreeSurfer software package and parcellated cortical and subcortical areas to 68 and 148 ROIs using the Desikan-Killiany atlas [44] and the Destrieux atlas [45], respectively. Then volumetric and surface measures, e.g. mean intensity and surface area of cortical and subcortical regions, were calculated. It is noteworthy that for each modality (rs-fMRI or sMRI), we first extracted features separately for each of two atlases that generated four sets of features corresponding to two modalities and two atlases per each modality. As listed in Table 2, we performed four single modality analyses in which one feature set for each of two modalities and two atlases were utilized. In multi-modal analyses, we concatenated two feature sets from two modalities, considering one atlas for each modality (see Table 2).

Filter and wrapper feature selection algorithms were used to select an optimal subset of features from sMRI volumetric and surface measures and rs-fMRI graph measures. To this end, we used the multivariate minimal redundancy maximal relevance (MRMR) feature selection algorithm to sort the features based on their individual discrimination ability. Next, we used our developed sequential features collection (SFC) algorithm to find an optimal subset of features. Later, we used SVM and the optimal subset of features to classify MCI-C from MCI-NC. In our previous studies for classification of AD and MCI, we compared the performances of various classifiers that have been used in bioinformatics literature, including SVM (with linear, polynomial, and RBF kernels), naïve Bayes, k-nearest neighbor, Fisher linear, linear discriminant, quadratic classifier, and decision tree [19,20]. We found that the SVM and naïve Bayes classifiers outperformed other classifiers and that SVM outperformed the naïve Bayes classifier [19]. It has been shown that SVM can achieve high classification accuracy with small training sample sizes compared to other classification algorithms [28]. Therefore, we used SVM in the current study. The k-fold cross-validation (KCV; $k = 9$) was employed to evaluate performance of SVM, separately for rs-fMRI (two atlases) and sMRI (two atlases), to classify MCI-C from MCI-NC, and to identify brain areas with significantly different features in MCI-C and MCI-NC groups. We also performed network-based statistics (NBS) analysis on rs-fMRI connectivity matrices to find brain networks with the most discriminative ability in predicting AD.

2.2. Patients

Data for this study were selected from the publicly available Alzheimer's disease neuroimaging initiative (ADNI) database.[2] The diagnosis of MCI patients in ADNI was based on cognitive tests like the Mini–Mental State Examination (MMSE) score, Activities of daily living, and the Clinical Dementia Rating (CDR) score. Eighteen MCI-C (11 male; 73.6 ± 15.7 (mean ± standard deviation) years of age) and 62 age-matched MCI-NC (28 male; 73.0 ± 16.3 (mean ± standard deviation) years of age) were included in this study (Table 1). The MCI-C patients were converted to AD after 6–36 months, and had MMSE scores of 24–28, a CDR score of 0.5, and Functional Activities Questionnaire (FAQ) scores of 1–22. We excluded the MCI-C patients who had a conversion from AD to MCI after their conversion from MCI to AD. The MCI-NC patients did not converted to AD after 36 months of follow-up, and had MMSE scores of 24–30, a CDR of 0.5, and FAQ scores of 0–18. All patients had no significant impairment in other cognitive domains, preserved activities of daily living, and an absence of dementia. It is noteworthy that all MCI-C and MCI-NC patients from the ADNI database who had rs-fMRI and sMRI data were included in this study.

Table 1
Demographic and clinical data.

	MCI converter	MCI non-converter	P-value
	(MCI-C)	(MCI-NC)	
Number	18	62	–
Male/Female	11/7	28/34	0.233
EMCI/LMCI	6/12	38/24	0.035
Age	73.6 ± 15.7	73.0 ± 16.3	0.256
MMSE score	26.0 ± 2.0	27 ± 3.0	0.056
CDR score	0.5 ± 0.0	0.5 ± 0.0	0.177
FAQ score	11.5 ± 10.5	9.0 ± 9.0	0.049

EMCI: Early MCI; LMCI: Late MCI.

2.3. Data acquisition and preprocessing

2.3.1. rs-fMRI

The functional and structural MRI images were collected using a 3-T Philips scanner. Acquisitions were performed according to the ADNI acquisition protocol [46]. A total of 140 functional volumes (TR/TE = 3000/30 ms, flip angle = 80°, slice thickness = 3.313 mm, 48 slices) were obtained. Participants were instructed to rest with their eyes open. For each subject, the first few volumes (7 vol) of fMRI data were discarded for signal equilibrium and to allow for the participant's adaptation to the experimental circumstances, leaving rest volumes for next steps [18]. Standard preprocessing was applied to the rs-fMRI dataset using Data Processing Assistant for Resting State fMRI (DPARSF) toolbox [47] and SPM12 package (http://www.fil.ion.ucl.ac.uk/spm). Slice-timing correction to the last slice was performed. The fMRI time series were realigned using a six-parameter rigid-body spatial transformation to compensate for head movement effects. Then all images were normalized into the Montreal Neurological Institute (MNI) space, resampled to 3-mm isotropic voxels, detrended, smoothed using a Gaussian filter with FWHM = 4 mm, and band-pass filtered (0.01–0.08 Hz). To reduce the effect of the physiological artifacts, the whole-brain signal was removed by a multiple linear regression analysis. In addition to the global mean signal, six head motion parameters, the cerebrospinal fluid (CSF), and the white matter signals were removed as nuisance covariates to reduce the effects of motion and non-neuronal blood oxygenation level-dependent (BOLD) fluctuations [48].

2.3.2. sMRI

The FreeSurfer image suite (http://surfer.nmr.mgh.harvard.edu) was used to generate regional cortical thickness and volumetric measures from the T1-weighted MRI of all subjects. The technical details for these procedures are described in prior publications listed online (https://surfer.nmr.mgh.harvard.edu/fswiki/FreeSurferMethodsCitation). Briefly, the processing includes removal of non-brain tissue using a hybrid watershed/surface deformation procedure [49]; automated Talairach transformation; segmentation of the

[2] Data used in the preparation of this article were obtained from the Alzheimer's Disease Neuroimaging Initiative (ADNI) database (adni.loni.usc.edu). The ADNI was launched in 2003 as a public-private partnership, led by Principal Investigator Michael W. Weiner, MD. The primary goal of ADNI has been to test whether serial magnetic resonance imaging (MRI), positron emission tomography (PET), other biological markers, and clinical and neuropsychological assessment can be combined to measure the progression of mild cognitive impairment (MCI) and early Alzheimer's disease (AD). For up-to-date information, see www.adni-info.org.

Table 2
Accuracy, sensitivity, specificity, positive predictive value (PPV), and AUC of SVM classifier in discriminating MCI-C from MCI-NC using a subset of optimal features, extracted from rs-fMRI and sMRI using different atlases. The classifier with maximum accuracy, shown in **bold** font, was based on the features extracted from rs-fMRI (Dosenbach atlas) and sMRI (Destrieux atlas).

Neuroimaging methods [Atlas]	No. of selected features	Accuracy (%)	Sensitivity (%)	Specificity (%)	PPV (%)	AUC
rs-fMRI [AAL]	10	91.40	83.24	90.1	84.22	0.94
rs-fMRI [Dosenbach]	8	93.04	93.15	93.08	92.96	0.89
sMRI [Destrieux]	32	89.41	91.40	87.97	87.28	0.91
sMRI [Desikan]	10	75.05	68.60	84.10	88.80	0.73
rs-fMRI [AAL] & sMRI [Destrieux]	27	92.97	91.69	93.37	93.36	0.98
rs-fMRI [AAL] & sMRI [Desikan]	11	92.39	88.91	98.16	98.28	0.92
rs-fMRI [Dosenbach] & sMRI [Destrieux]	**6**	**96.97**	**94.97**	**100**	**100**	**0.98**
rs-fMRI [Dosenbach] & sMRI [Desikan]	11	94.46	90.82	98.92	98.97	0.93

subcortical deep gray matter and white matter volumetric structures [49–51]; intensity normalization; tessellation of gray matter and white matter boundary; automated topology correction [52]; and deformation following intensity gradients to optimally place the gray/white and gray/cerebrospinal fluid borders at the location where the greatest shift in intensity defines the transition to the other tissue class [53,54]. After completing the cortical models, deformable procedures were performed for further data processing, including surface inflation and registration to a spherical atlas [55], parcellation of the cerebral cortex [56], and creation of a variety of surface-based measures including surface area, curvatures, and volumes. In this study, we used two atlases for sMRI parcellation: the Destrieux atlas (74 areas in each hemisphere) [56], and the Desikan-Killiany atlas (34 areas in each hemisphere) [44].

2.4. Extracting features from rs-fMRI and sMRI data

The rs-fMRI features were constructed based on graph theory and the connectivity matrix. We used the AAL (90 ROIs) and Dosenbach atlases (160 ROIs) and calculated a connectivity matrix for each subject using the average of the Pearson's correlation between the time series of the BOLD signals of all voxels within the ROIs. Similar to our previous studies [17–20], we converted the weighted connectivity matrices to binary ones by applying an optimal threshold on the connectivity matrices [57,58]. As described in Ref. [57], the optimal threshold maximizes the global cost efficiency (GCE) of the brain network. By changing the ratio of the retained strong connections to the total number of connections (defined as cost) from 0 to 1, we investigated finding an optimal cost that maximizes the GCE for each patient. The optimal values of costs were 18.8% ± 3.0% (mean ± STD) and 19.7% ± 2.4% across patients in MCI-C and MCI-NC groups, respectively. To have the same number of connections after thresholding in all patients, we retained 19.2% of the strongest weights of the connectivity matrices of all patients, and then computed the graph measures.

The GraphVar (Version 6.2) toolbox was employed for computing 10 local and 13 global graph measures [59]. The local graph measures were: betweenness centrality, clustering coefficient, characteristic path, community structure Newman, community structure Louvain, eccentricity, eigenvector centrality, rich club coefficient, subgraph centrality [60], and participation coefficient [61]. The global graph measures were: assortativity, clustering coefficient, characteristic path, community structure Newman output, community structure Louvain output, cost efficiency (relative threshold), cost efficiency (absolute threshold), density, efficiency, graph radius, graph diameter, transitivity, and small-worldness [61].

Volumes of the subcortical structures and surface area, curvature, thickness, and volume of cortical areas were considered as sMRI features in our algorithm. The FreeSurfer pipeline generated 45 regional subcortical volumes, and we excluded 11 vol corresponding to the optic chiasm, right and left choroid plexus, right and left vessel, and white matter hypointensities from our analysis. We used the Destrieux (148 ROIs) and Desikan-Killiany (68 ROIs) atlases for parcellation of the cortical areas. For each cortical ROI, volume of gray matter, surface area, average and standard deviation of thickness, and average of curvature were considered as sMRI features in our algorithm.

In neurodegeneration studies, normalization of regional brain volumes and cortical surface is frequently performed in order to enhance estimation of the extent of atrophy that is caused by pathology and is not a consequence of gender differences or other factors [62]. For anatomical normalization of each subject in this study, the volumes of cortical ROIs and subcortical structures were divided by the corresponding estimated intracranial volume (eTIV), and the surface areas of cortical ROIs were divided by total area of the same hemisphere [38,63].

2.5. Feature selection and classification

A feature selection algorithm is the essential part of a machine learning approach, which facilitates data understanding, reduces the storage requirements and training-testing times, and improves accuracy of classification. We used a combination of filter and wrapper algorithms for feature selection. We used a filter method and sorted features based on their MRMR scores [64]. The MRMR score for a feature set S is defined as:

$$MRMR = MAX_S\left\{\frac{1}{|S|}\sum_{f_i \varepsilon S} I(f_i; c) - \frac{1}{|S|^2}\sum_{f_i, f_j \varepsilon S} I(f_i; f_j)\right\} \quad (1)$$

where the relevance of a feature set S for k classes $C = \{c_1, c_2, \ldots, c_k\}$ is defined by the average value of mutual information between the individual feature f_i and C, and the redundancy of all features in the feature set S is the average value of mutual information between features f_i and f_j. The top 50 features identified by the MRMR algorithm were used in a wrapper algorithm with the SVM classifier to find an optimal subset of features. The SVM classifier has been successfully used in the previous AD studies [17–20,65], and we utilized this classifier in the current study. The SVM was implemented in MATLAB (The Math Works, Natwick, MA) and LIBSVM (http://www.csie.ntu.edu.tw/cjlin/libsvm/). We observed that SVM with linear and non-linear kernels provided a similar calcification accuracy. Considering the simplicity of the SVM with the linear kernel and also the fact that solving the optimization problem for the linear kernel is much faster than that for the non-linear kernel [66], we utilized SVM with the linear kernel in this study.

We developed and validated a sequential features collection (SFC) algorithm as a wrapper feature selection and a classification method in our previous study [22], and we used this algorithm in the current study. The SFC algorithm was described in detail previously [22]. Briefly, different subsets of features were selected within the top 50 features identified by the MRMR algorithm, then the accuracy of the SVM classifiers based on these subsets of features were calculated using the KCV ($k = 9$) cross-validation approach. In each fold of KCV, 90% of data were used to train the model based on a subset of features, then

10% of data (cross-validation set) were used to calculate accuracy of the SVM classifier. Accuracies of the SVM classifiers corresponding to all subsets of features were calculated and classifiers with maximum accuracy and the corresponding optimal subset of features were identified. Since SVM with unequal class sizes (in this study 18 MCI-C and 62 MCI-NC) can lead to a biased accuracy of classification, we used a repeated random sub-sampling method to overcome this issue. We randomly selected 18 out of 62 MCI-NC patients and evaluated performance of the SVM using those selected MCI-NC patients and 18 MCI-C patients using the KCV ($k = 9$). The random sub-sampling of MCI-NC patients was repeated 1000 times, and the average accuracy, sensitivity, specificity, positive predictive value, and the AUC across this repetition were calculated.

2.6. Network-based statistics (NBS)

We performed NBS on the weighted rs-fMRI connectivity matrices [67]. In the NBS methodology, a *t*-test was first performed independently for each connection in the network to test the null hypothesis for equality of the mean value of that connection in two groups (MCI-C and MCI-NC). Connections with a *t*-value above a primary threshold contain a supra-threshold connection set. The connectivity matrix was then searched for any connected graph components defined by the set of supra-threshold connections, and the sizes of those connected components were calculated. Then permutation testing ($n = 10{,}000$) was performed by assigning subjects randomly to a group (either MCI-C or MCI-NC) to find an empirical null distribution for the size of the largest connected component. Finally, the family-wise error rate corrected *p*-value for a given component size was calculated, and used to identify components that were significantly different in the two groups (MCI-C and MCI-NC).

3. Results

3.1. Discrimination of patients with MCI-C and MCI-NC

Performances of eight SVM classifiers for separating MCI-C from MCI-NC using a subset of rs-fMRI and/or sMRI features, based on two atlases for each modality, are compared in Table 2. Results in Table 2 reveal that the best classifier was based on integrated rs-fMRI (Dosenbach) and sMRI (Destrieux) features and the worst classifier was based on sMRI (Desikan-Killiany atlas) features. The best classifier for separating MCI-C from MCI-NC was based on a combination of six rs-fMRI and sMRI features. This classifier achieved an accuracy, sensitivity, specificity, positive predictive value (PPV), and AUC of 97.0%, 95.0%, 100%, 100%, and 0.98, respectively (Table 2). By utilizing only the sMRI features, the best accuracy of 89.4% was achieved using the Destrieux atlas. By using only the rs-fMRI features, the best accuracy of 93.0% was achieved using the Dosenbach atlas.

In Table 3, six features corresponding to the best classifier, i.e., a classifier with a combination of rs-fMRI (Dosenbach atlas) and sMRI (Destrieux atlas) features, are listed. Of those six features, four were rs-fMRI graph measures and two were sMRI features. The characteristic path (a global graph measure) of MCI-C was significantly larger than that of MCI-NC ($p < 1.6 \times 10^{-7}$). Three local rs-fMRI graph measures, i.e. clustering coefficient in precuneus, rich club coefficient in dorsolateral prefrontal cortex (dlPFC), and eigenvector centrality in occipital, were also significantly different in the two groups ($p < 1.4 \times 10^{-3}$). The average of cortical thickness of the left superior temporal sulcus (LSTS) and the surface area of right inferior temporal gyrus (RITG), as sMRI features, were significantly smaller in MCI-C than in MCI-NC ($p < 1.9 \times 10^{-4}$) subjects. Locations of the cortical areas corresponding to three local rs-fMRI graph measures and two sMRI features are shown in Fig. 2.

3.2. Network-based statistical analysis

We performed NBS on the weighted raw rs-fMRI connectivity matrices to identify impaired sub-networks in patients with MCI-C and MCI-NC [67]. By applying NBS on the raw connectivity matrices, generated using the Dosenbach atlas, we identified three networks that were significantly different in the two groups (Fig. 3). These networks were identified using a threshold at $t = 7.38$ (*p*-value < 0.001, corrected for multiple comparisons). The first network comprised two edges (i.e., connections) and three nodes (i.e., brain regions). One node of this network was within the precuneus and other two nodes were within the cerebellum. The second network comprised three edges and four nodes within the ventral prefrontal cortex (vPFC), anterior insula, ventral frontal cortex (VFC), and occipital. The third network comprised two edges and three nodes within the temporoparietal junction (TPJ), occipital, and lateral cerebellum.

4. Discussion

We compared the performances of single modality (i.e. fMRI or sMRI) and two-modality approaches for prediction of the early stage of AD. For the single modality approach, sMRI with the Desikan-Killiany atlas provided the worst performance (75% accuracy and 0.73 AUC) and rs-fMRI with the Dosenbach atlas achieved the best performance (93% accuracy and 0.89 AUC). While the performance of rs-fMRI with the Dosenbach atlas was slightly better than that with the AAL atlas, the performance of sMRI was highly improved using the Destrieux atlas (89% accuracy) compared to that using the Desikan-Killiany atlas (75% accuracy). The superior performances obtained from utilizing the Dosenbach and Destrieux atlases are expected since these atlases parcellated the brain regions to finer parcels compared to the AAL and Desikan-Killiany atlases. In fact, the Dosenbach and Destrieux atlases included twice the number of ROIs compared to the AAL and Desikan-Killiany atlases.

Our results revealed that the performances of rs-fMRI and sMRI for prediction of the early stage of AD are comparable, although rs-fMRI had a slightly superior performance compared to sMRI (Table 2). In agreement with previous studies [68], our results show that biomarkers based on fMRI hold promise for early detection and differential diagnosis of AD and for predicting future alteration in patients with MCI. It was reported that synaptic dysfunction occurs in patients with AD, and

Table 3
Optimal six rs-fMRI and sMRI features which were selected by SFC algorithm. The rs-fMRI and sMRI features correspond to the Dosenbach and Destrieux atlases, respectively. *P*-values show the results of *t*-test for the difference of the features in two groups (MCI-C and MCI-NC).

Imaging	Features	Type of feature	Brain regions	MCI-C (mean ± STD)	MCI-NC (mean ± STD)	*p*-value
rs-fMRI	Characteristic path	graph (global)	–	1.112 ± 0.026	1.095 ± 0.031	$\mathbf{1.58 \times 10^{-7}}$
rs-fMRI	Clustering coefficient	graph (local)	Precuneus_L	1.650 ± 0.337	2.318 ± 0.510	$\mathbf{5.26 \times 10^{-5}}$
rs-fMRI	Rich club coefficient	graph (local)	dlPFC_R	1.013 ± 0.007	1.003 ± 0.003	$\mathbf{2.30 \times 10^{-4}}$
rs-fMRI	Eigenvector centrality	graph (local)	Occipital_L	1.028 ± 0.194	0.757 ± 0.316	$\mathbf{1.34 \times 10^{-3}}$
sMRI	Average of cortical thickness	structural	S_temporal_sup_L	2.123 ± 0.118	2.281 ± 0.118	$\mathbf{1.15 \times 10^{-5}}$
sMRI	Cortical area	structural	G_temporal_inf_R	0.015 ± 0.006	0.019 ± 0.002	$\mathbf{1.90 \times 10^{-4}}$

dlPFC: Dorsolateral prefrontal cortex; S_temporal_sup_L: Left superior temporal sulcus (parallel sulcus); G_temporal_inf_R: Right inferior temporal gyrus.

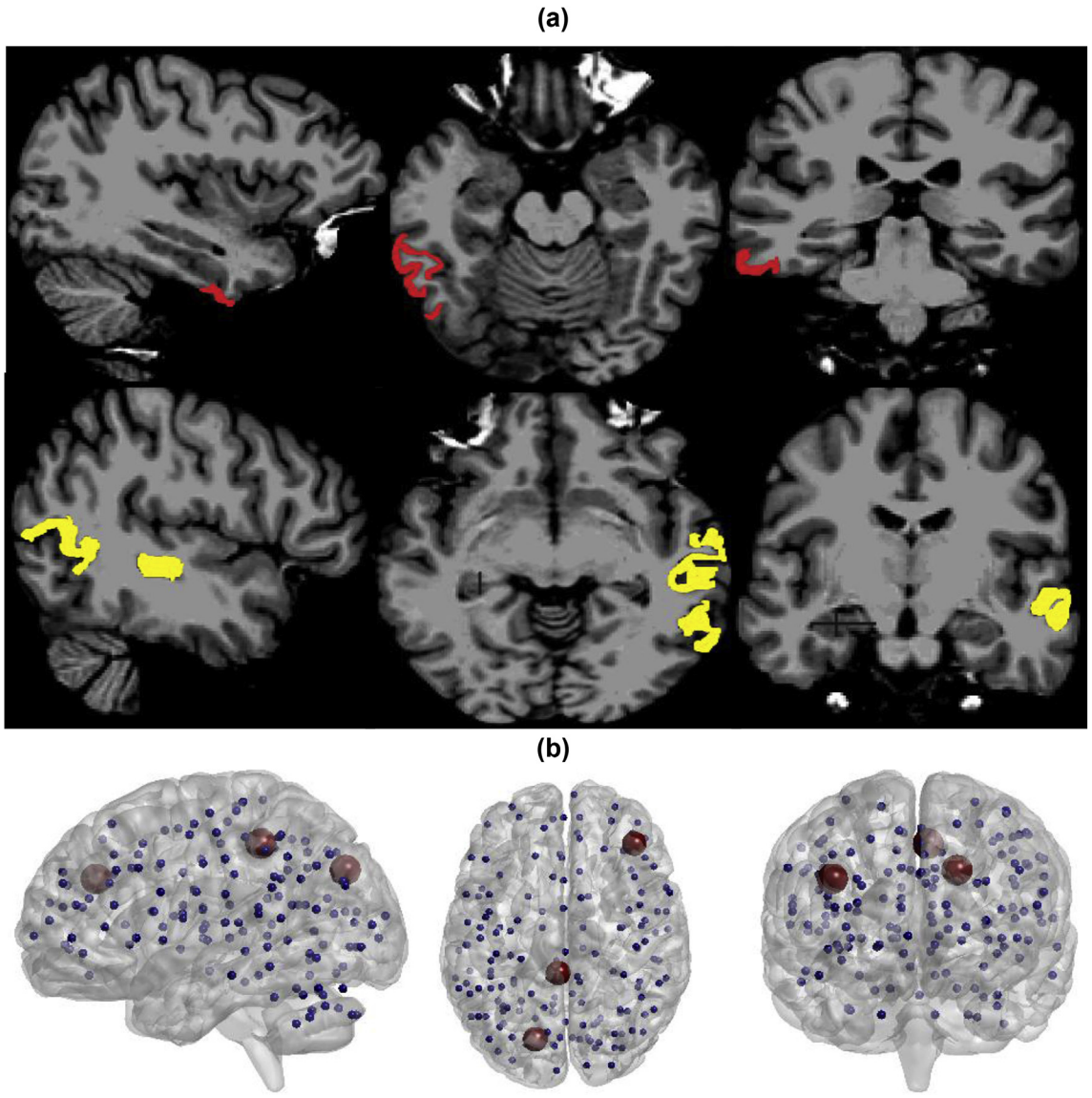

Fig. 2. (a) Locations of two cortical regions: left superior temporal sulcus (LSTS) and right inferior temporal gyrus (RITG), with highly discriminative sMRI features (Table 3). The RITG and LSTS are marked by red and yellow colors, respectively. (b) Locations of three cortical areas, i.e., precuneus, dlPFC, and occipital, with highly discriminative rs-fMRI features (Table 3). (For interpretation of the references to color in this figure legend, the reader is referred to the Web version of this article.)

this dysfunction is highly correlated to cognitive decline in AD [69]. Considering synaptic dysfunction and loss in the early stage of AD, it is expected that biomarkers based on connectivity may outperform biomarkers based on structural changes in identification of the early stage of the disease [69,70]. In agreement with this expectation, our results in Table 2 show that rs-fMRI was more sensitive than sMRI in identification of AD progress.

The results of this study confirmed our expectation that integrating two modalities surpasses the performance of the single modality approach (Table 2). By integrating two modalities, not only was the performance of MCI-C versus MCI-NC classification improved, but we also achieved a perfect specificity by integrating features extracted from rs-fMRI (Dosenbach atlas) and sMRI (Destrieux atlas). Our findings are in agreement with previous studies in MCI and AD, although no study has yet investigated integrating sMRI with rs-fMRI for prediction of the early stage of AD. In agreement with the current study, a few previous studies reported that integrating sMRI with rs-fMRI improved the performance of classifying AD from controls [39,40]. However, our results are in contrast with findings of a previous study reporting that integrating sMRI with rs-fMRI did not improve the performance of classifying AD from controls [38]. The difference between results of the current study and those of Dyrba et al. is possibly explained by the efficiency of our SFC feature selection algorithm. While Dyrba et al. used a large number of features in classification, our SFC algorithm found a small number of efficient features. It is worth mentioning that integration of sMRI with rs-fMRI increases the number of features, and if the feature selection algorithm does not work appropriately, the integrated approach can result in an inferior performance because of using a larger number of redundant features. A larger number of redundant features can cause an overfitting in the training, thus reducing performance in testing. Our SFC algorithm worked very well in identifying and removing redundant features. For instance, the SFC algorithm selected 8 and 32 features for rs-fMRI (Dosenbach atlas) and sMRI (Destrieux atlas), respectively, in the single modality approach, while this algorithm selected only 6 optimal features in the combination of two modalities, by removing all redundant features and keeping only a few informative features.

Previous sMRI studies investigated the prediction of the early stage

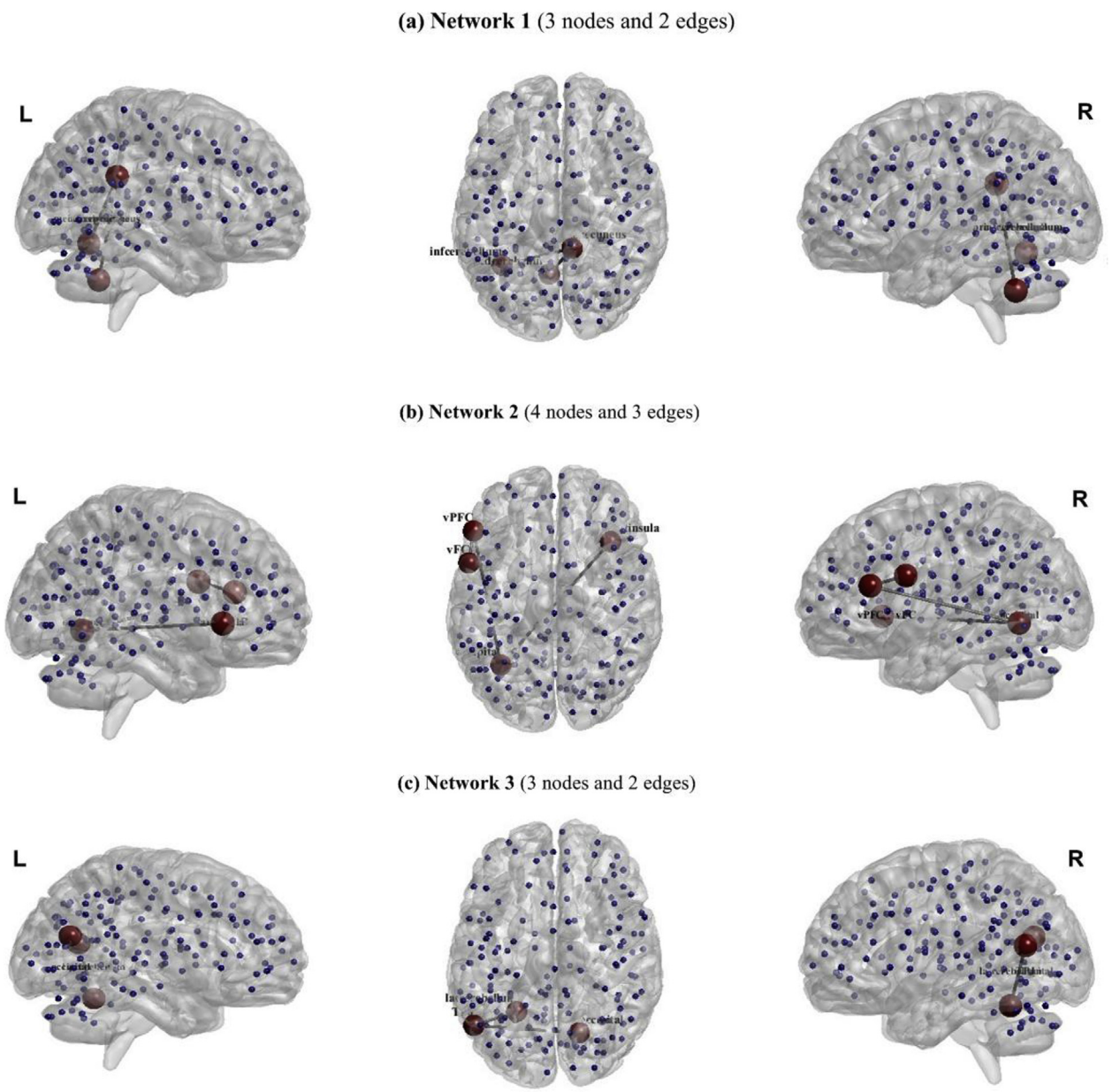

Fig. 3. Three rs-fMRI brain networks that were significantly different in MCI-C and MCI-NC based on the network-based statistics (NBS) analysis. Dosenbach atlas was used for the parcellation of the brain regions in the NBS analysis. List of nodes, i.e., cortical areas, of these networks are as follows.
(a) Network 1: middle cerebellar peduncle, inferior cerebellar peduncle, and precuneus cortex. (b) Network 2: ventral prefrontal cortex (vPFC), anterior insula, ventral frontal cortex (VFC), and occipital. (c) Network 3: temporoparietal junction (TPJ), lateral cerebellum, and occipital.

of AD and reported a wide range of accuracy, from 59% to 82%, for differentiating MCI-C from MCI-NC [6–8,71,72] (Especially see Moradi et al. [71] for a nice comparison of the performances of sMRI studies.). In a previous sMRI study, Eskildsen et al. [6] used patterns of cortical thickness and identified cortical regions potentially discriminative for distinguishing MCI-C from MCI-NC. They considered time to conversion from MCI to AD and defined four groups of MCI-C patients corresponding to the time to conversion of 6, 12, 24, and 36 months. They reported that the accuracy of classifying MCI-C from MCI-NC declined as the time to conversion from MCI to AD increased, from 76% at 6 months before the clinical criteria for AD was met, to 70% at 36 months before AD. The MCI-C patients in the current study had a time to conversion from MCI to AD of 6–36 months, and we considered all of these patients in one group to test performance of our algorithm in a more challenging condition compared to that used in Ref. [6]. Our algorithm based on sMRI and the Destrieux atlas provided an accuracy of 89%, better than the best accuracy of 76% reported by Eskildsen and his colleagues. It is noteworthy that while previous studies have investigated the utility of sMRI for classification of MCI-C from MCI-NC, application of rs-fMRI for this classification has not been explored thoroughly. In fact, our previous work was the first study that used rs-fMRI based on the AAL atlas parcellation for classification of MCI-C from MCI-NC, and we achieved an accuracy of 91.4% [22]. In the current study, we improved the performance of rs-fMRI by using the Dosenbach atlas and integrated this modality with sMRI.

As listed in Table 3, the best classifier for separating MCI-C from MCI-NC patients was based on four rs-fMRI graph measures and two structural MRI features. The rs-fMRI graph measures included one global measure and three local measures in three areas, i.e., precuneus, dlPFC, and occipital. In agreement with our findings, these areas have previously been found to be highly discriminative for AD [73,74]. The eigenvector centrality, rich club coefficient, and clustering coefficient

were local rs-fMRI graph measures that selected by the SFC algorithm for classifying MCI-C from MCI-NC. It is noteworthy that the rich club coefficient in dlPFC and the clustering coefficient in precuneus were significantly different in MCI-C versus MCI-NC (Table 3). In agreement with our results, previous studies have reported that these graph measures are highly discriminative for AD [75,76]. Two sMRI features, i.e. average cortical thickness of the left superior temporal sulcus and surface area of the right inferior temporal gyrus, were selected by the SFC algorithm to be used in the best classifier (Table 3). Our findings are in agreement with previous studies reporting that these features were discriminative for AD [77–80].

Using the Dosenbach atlas and NBS analysis, we identified three rs-fMRI networks that were significantly different in MCI-C and MCI-NC (Fig. 3). The first network was comprised of two edges and three nodes (i.e., brain regions). In this network, precuneus was connected to the middle and inferior cerebellar peduncles. The precuneus plays an essential role in the default mode network. In agreement with our finding for involvement of precuneus in AD, previous studies reported the existence of disproportionate atrophy in the precuneus in patients with early-onset AD [81]. The second network comprised three edges in four regions: anterior insula, vPFC, VFC, and occipital cortex. The insular cortex is involved in a range of regulatory mechanisms from visceral control to covert judgments [82]. The dementia of AD usually consists of visceral dysfunction and behavioral dyscontrol that may be related to autonomic instability and to loss of the sense of self. Therefore, insula cortex was reported to play an essential role in AD [82–84]. Our finding for association of the occipital cortex in the early stage of AD is in agreement with previous studies reporting that atrophy spread to the lateral occipital cortex by increasing impairment in MCI patients [85,86]. In the third network, the TPJ was connected to the lateral cerebellum and occipital cortex. Consistent with our findings, previous studies demonstrated association of the TPJ to AD [25,87]. The TPJ is part of the associative cortices, where metabolism is typically impaired in AD [25]. It was reported that the global dementia scores are related to decreased metabolism in TPJ in patients with AD [87].

5. Conclusion

We developed and evaluated a machine learning approach to compare and integrate rs-fMRI and sMRI features for classification of MCI-C from MCI-NC. We developed eight classifiers by considering the rs-fMRI features (corresponding to two atlases), s-MRI features (corresponding to two atlases), or combination of the rs-fMRI and sMRI features (four classifiers corresponding to two atlases for each modality). We then utilized our SFC algorithm to select optimal small subsets of features for each classifier. The classifiers were trained and cross-validated, and their performances were compared. We found that the best classifier for distinguishing MCI-C from MCI-NC was based on a combination of six rs-fMRI and sMRI features. This classifier achieved an accuracy of 97% and an AUC of 0.98. Our findings revealed that integration of rs-fMRI and sMRI can improve the performance of identification of the early stage of AD compared to a single modality approach.

Compliance with ethical standards

Study funding

This study was supported by the Children's Foundation Research Institute at Le Bonheur Children's Hospital and the Le Bonheur Associate Board, Memphis, TN.

Conflict of interest

The authors declare that they have no conflicts of interest.

Ethical approval

"All procedures performed in studies involving human participants were in accordance with the ethical standards of the institutional and/or national research committee and with the 1964 Helsinki declaration and its later amendments or comparable ethical standards."

Informed consent

As part of ADNI protocol, informed consent was obtained from all participants and/or authorized representatives and the study partners.

Acknowledgments

Data used in this paper were obtained from the Alzheimer's Disease Neuroimaging Initiative (ADNI) database (http://ADNI.loni.usc.edu). The investigators within the ADNI, who can be found at http://ADNI.loni.usc.edu/study-design/ongoing-investigations, contributed to the design and implementation of ADNI and/or provided data but did not participate in analysis or the writing of this article. Data collection and sharing for this project was funded by the Alzheimer's Disease Neuroimaging Initiative (National Institutes of Health Grant U01 AG024904). ADNI is funded by the National Institute on Aging, the National Institute of Biomedical Imaging and Bioengineering, and through generous contributions from the following: AbbVie, Alzheimer's Association; Alzheimer's Drug Discovery Foundation; Araclon Biotech; BioClinica, Inc.; Biogen; Bristol-Myers Squibb Company; CereSpir, Inc.; Eisai Inc.; Elan Pharmaceuticals, Inc.; Eli Lilly and Company; EuroImmun; F. Hoffmann-La Roche Ltd and its affiliated company Genentech, Inc.; Fujirebio; GE Healthcare; IXICO Ltd.; Janssen Alzheimer Immunotherapy Research & Development, LLC.; Johnson & Johnson Pharmaceutical Research & Development LLC.; Lumosity; Lundbeck; Merck & Co., Inc.; Meso Scale Diagnostics, LLC.; NeuroRx Research; Neurotrack Technologies; Novartis Pharmaceuticals Corporation; Pfizer Inc.; Piramal Imaging; Servier; Takeda Pharmaceutical Company; and Transition Therapeutics. The Canadian Institutes of Health Research is providing funds to support ADNI clinical sites in Canada. Private sector contributions are facilitated by the Foundation for the National Institutes of Health (www.fnih.org). The grantee organization is the Northern California Institute for Research and Education, and the study is coordinated by the Alzheimer's Disease Cooperative Study at the University of California, San Diego. ADNI data are disseminated by the Laboratory for Neuro Imaging at the University of Southern California.

References

[1] R.C. Petersen, R. Doody, A. Kurz, R.C. Mohs, J.C. Morris, P.V. Rabins, K. Ritchie, M. Rossor, L. Thal, B. Winblad, Current concepts in mild cognitive impairment, Arch. Neurol. 58 (2001) 1985–1992.

[2] A.L. Bokde, P. Lopez-Bayo, T. Meindl, S. Pechler, C. Born, F. Faltraco, S.J. Teipel, H.J. Moller, H. Hampel, Functional connectivity of the fusiform gyrus during a face-matching task in subjects with mild cognitive impairment, Brain 129 (2006) 1113–1124.

[3] K.R. Gray, P. Aljabar, R.A. Heckemann, A. Hammers, D. Rueckert, I. Alzheimer's Disease Neuroimaging, Random forest-based similarity measures for multi-modal classification of Alzheimer's disease, Neuroimage 65 (2013) 167–175.

[4] J.L. Whitwell, M.M. Shiung, S.A. Przybelski, S.D. Weigand, D.S. Knopman, B.F. Boeve, R.C. Petersen, C.R. Jack Jr., MRI patterns of atrophy associated with progression to AD in amnestic mild cognitive impairment, Neurology 70 (2008) 512–520.

[5] D. Zhang, Y. Wang, L. Zhou, H. Yuan, D. Shen, I. Alzheimer's Disease Neuroimaging, Multimodal classification of Alzheimer's disease and mild cognitive impairment, Neuroimage 55 (2011) 856–867.

[6] S.F. Eskildsen, P. Coupe, D. Garcia-Lorenzo, V. Fonov, J.C. Pruessner, D.L. Collins, I. Alzheimer's Disease Neuroimaging, Prediction of Alzheimer's disease in subjects with mild cognitive impairment from the ADNI cohort using patterns of cortical thinning, Neuroimage 65 (2013) 511–521.

[7] C. Misra, Y. Fan, C. Davatzikos, Baseline and longitudinal patterns of brain atrophy in MCI patients, and their use in prediction of short-term conversion to AD: results from ADNI, Neuroimage 44 (2009) 1415–1422.

[8] R. Wolz, V. Julkunen, J. Koikkalainen, E. Niskanen, D.P. Zhang, D. Rueckert, H. Soininen, J. Lotjonen, I. Alzheimer's Disease Neuroimaging, Multi-method analysis of MRI images in early diagnostics of Alzheimer's disease, PLoS One 6 (2011) e25446.
[9] F. de Vos, T.M. Schouten, A. Hafkemeijer, E.G. Dopper, J.C. van Swieten, M. de Rooij, J. van der Grond, S.A. Rombouts, Combining multiple anatomical MRI measures improves Alzheimer's disease classification, Hum. Brain Mapp. 37 (2016) 1920–1929.
[10] M.M. Mesulam, Some cholinergic themes related to Alzheimer's disease: synaptology of the nucleus basalis, location of m2 receptors, interactions with amyloid metabolism, and perturbations of cortical plasticity, J. Physiol. Paris 92 (1998) 293–298.
[11] A.S. Fleisher, A. Sherzai, C. Taylor, J.B. Langbaum, K. Chen, R.B. Buxton, Resting-state BOLD networks versus task-associated functional MRI for distinguishing Alzheimer's disease risk groups, Neuroimage 47 (2009) 1678–1690.
[12] Y. He, Z.J. Chen, A.C. Evans, Small-world anatomical networks in the human brain revealed by cortical thickness from MRI, Cerebr. Cortex 17 (2007) 2407–2419.
[13] S.A. Rombouts, F. Barkhof, R. Goekoop, C.J. Stam, P. Scheltens, Altered resting state networks in mild cognitive impairment and mild Alzheimer's disease: an fMRI study, Hum. Brain Mapp. 26 (2005) 231–239.
[14] C. Sorg, V. Riedl, M. Muhlau, V.D. Calhoun, T. Eichele, L. Laer, A. Drzezga, H. Forstl, A. Kurz, C. Zimmer, A.M. Wohlschlager, Selective changes of resting-state networks in individuals at risk for Alzheimer's disease, Proc. Natl. Acad. Sci. U. S. A. 104 (2007) 18760–18765.
[15] K. Supekar, V. Menon, D. Rubin, M. Musen, M.D. Greicius, Network analysis of intrinsic functional brain connectivity in Alzheimer's disease, PLoS Comput. Biol. 4 (2008) e1000100.
[16] M. Bozzali, A. Padovani, C. Caltagirone, B. Borroni, Regional grey matter loss and brain disconnection across Alzheimer disease evolution, Curr. Med. Chem. 18 (2011) 2452–2458.
[17] A. Khazaee, A. Ebrahimzadeh, A. Babajani-Feremi, Application of pattern recognition and graph theoretical approaches to analysis of brain network in Alzheimer's disease, J. Med. Imaging Health Inform. 5 (2015) 1145–1155.
[18] A. Khazaee, A. Ebrahimzadeh, A. Babajani-Feremi, Identifying patients with Alzheimer's disease using resting-state fMRI and graph theory, Clin. Neurophysiol. 126 (2015) 2132–2141.
[19] A. Khazaee, A. Ebrahimzadeh, A. Babajani-Feremi, Application of advanced machine learning methods on resting-state fMRI network for identification of mild cognitive impairment and Alzheimer's disease, Brain Imaging Behav. 10 (2016) 799–817.
[20] A. Khazaee, A. Ebrahimzadeh, A. Babajani-Feremi, I. Alzheimer's Disease Neuroimaging, Classification of patients with MCI and AD from healthy controls using directed graph measures of resting-state fMRI, Behav. Brain Res. 322 (2017) 339–350.
[21] C.J. Stam, B.F. Jones, G. Nolte, M. Breakspear, P. Scheltens, Small-world networks and functional connectivity in Alzheimer's disease, Cerebr. Cortex 17 (2007) 92–99.
[22] S.H. Hojjati, A. Ebrahimzadeh, A. Khazaee, A. Babajani-Feremi, I. Alzheimer's Disease Neuroimaging, Predicting conversion from MCI to AD using resting-state fMRI, graph theoretical approach and SVM, J. Neurosci. Meth. 282 (2017) 69–80.
[23] J.C. Baron, G. Chetelat, B. Desgranges, G. Perchey, B. Landeau, V. de la Sayette, F. Eustache, In vivo mapping of gray matter loss with voxel-based morphometry in mild Alzheimer's disease, Neuroimage 14 (2001) 298–309.
[24] G.B. Frisoni, C. Testa, A. Zorzan, F. Sabattoli, A. Beltramello, H. Soininen, M.P. Laakso, Detection of grey matter loss in mild Alzheimer's disease with voxel based morphometry, J. Neurol. Neurosurg. Psychiatry 73 (2002) 657–664.
[25] K. Herholz, E. Salmon, D. Perani, J.C. Baron, V. Holthoff, L. Frolich, P. Schonknecht, K. Ito, R. Mielke, E. Kalbe, G. Zundorf, X. Delbeuck, O. Pelati, D. Anchisi, F. Fazio, N. Kerrouche, B. Desgranges, F. Eustache, B. Beuthien-Baumann, C. Menzel, J. Schroder, T. Kato, Y. Arahata, M. Henze, W.D. Heiss, Discrimination between Alzheimer dementia and controls by automated analysis of multicenter FDG PET, Neuroimage 17 (2002) 302–316.
[26] J.B. Langbaum, K. Chen, W. Lee, C. Reschke, D. Bandy, A.S. Fleisher, G.E. Alexander, N.L. Foster, M.W. Weiner, R.A. Koeppe, W.J. Jagust, E.M. Reiman, I. Alzheimer's Disease Neuroimaging, Categorical and correlational analyses of baseline fluorodeoxyglucose positron emission tomography images from the Alzheimer's Disease Neuroimaging Initiative (ADNI), Neuroimage 45 (2009) 1107–1116.
[27] D. Medina, L. DeToledo-Morrell, F. Urresta, J.D.E. Gabrieli, M. Moseley, D. Fleischman, D.A. Bennett, S. Leurgans, D.A. Turner, G.T. Stebbins, White matter changes in mild cognitive impairment and AD: a diffusion tensor imaging study, Neurobiol. Aging 27 (2006) 663–672.
[28] S. Rathore, M. Habes, M.A. Iftikhar, A. Shacklett, C. Davatzikos, A review on neuroimaging-based classification studies and associated feature extraction methods for Alzheimer's disease and its prodromal stages, Neuroimage 155 (2017) 530–548.
[29] S.E. Rose, K.L. McMahon, A.L. Janke, B. O'Dowd, G. de Zubicaray, M.W. Strudwick, J.B. Chalk, Diffusion indices on magnetic resonance imaging and neuropsychological performance in amnestic mild cognitive impairment, J. Neurol. Neurosurg. Psychiatry 77 (2006) 1122–1128.
[30] S. Teipel, M.J. Grothe, J. Zhou, J. Sepulcre, M. Dyrba, C. Sorg, C. Babiloni, Measuring cortical connectivity in Alzheimer's disease as a brain neural network pathology: toward clinical applications, J. Int. Neuropsychol. Soc. 22 (2016) 138–163.
[31] T. Tong, K. Gray, Q. Gao, L. Chen, D. Rueckert, A.s.D.N. Initiative, Multi-modal classification of Alzheimer's disease using nonlinear graph fusion, Pattern Recogn. 63 (2017) 171–181.
[32] M.R. Arbabshirani, S. Plis, J. Sui, V.D. Calhoun, Single subject prediction of brain disorders in neuroimaging: promises and pitfalls, Neuroimage 145 (2017) 137–165.
[33] C. Hinrichs, V. Singh, G. Xu, S.C. Johnson, I. Alzheimers Disease Neuroimaging, Predictive markers for AD in a multi-modality framework: an analysis of MCI progression in the ADNI population, Neuroimage 55 (2011) 574–589.
[34] C. Babiloni, C. Del Percio, M. Boccardi, R. Lizio, S. Lopez, F. Carducci, N. Marzano, A. Soricelli, R. Ferri, A.I. Triggiani, A. Prestia, S. Salinari, P.E. Rasser, E. Basar, F. Fama, F. Nobili, G. Yener, D.D. Emek-Savas, L. Gesualdo, C. Mundi, P.M. Thompson, P.M. Rossini, G.B. Frisoni, Occipital sources of resting-state alpha rhythms are related to local gray matter density in subjects with amnesic mild cognitive impairment and Alzheimer's disease, Neurobiol. Aging 36 (2015) 556–570.
[35] R.L. Strijers, P. Scheltens, E.J. Jonkman, W. de Rijke, C. Hooijer, C. Jonker, Diagnosing Alzheimer's disease in community-dwelling elderly: a comparison of EEG and MRI, Dement. Geriatr. Cognit. Disord. 8 (1997) 198–202.
[36] D.V. Moretti, G.B. Frisoni, C. Fracassi, M. Pievani, C. Geroldi, G. Binetti, P.M. Rossini, O. Zanetti, MCI patients' EEGs show group differences between those who progress and those who do not progress to AD, Neurobiol. Aging 32 (2011) 563–571.
[37] D.V. Moretti, C. Miniussi, G.B. Frisoni, C. Geroldi, O. Zanetti, G. Binetti, P.M. Rossini, Hippocampal atrophy and EEG markers in subjects with mild cognitive impairment, Clin. Neurophysiol. 118 (2007) 2716–2729.
[38] M. Dyrba, M. Grothe, T. Kirste, S.J. Teipel, Multimodal analysis of functional and structural disconnection in Alzheimer's disease using multiple kernel SVM, Hum. Brain Mapp. 36 (2015) 2118–2131.
[39] T.M. Schouten, M. Koini, F. de Vos, S. Seiler, J. van der Grond, A. Lechner, A. Hafkemeijer, C. Moller, R. Schmidt, M. de Rooij, S.A. Rombouts, Combining anatomical, diffusion, and resting state functional magnetic resonance imaging for individual classification of mild and moderate Alzheimer's disease, Neuroimage Clin. 11 (2016) 46–51.
[40] Z. Dai, C. Yan, Z. Wang, J. Wang, M. Xia, K. Li, Y. He, Discriminative analysis of early Alzheimer's disease using multi-modal imaging and multi-level characterization with multi-classifier (M3), Neuroimage 59 (2012) 2187–2195.
[41] F. Falahati, E. Westman, A. Simmons, Multivariate data analysis and machine learning in Alzheimer's disease with a focus on structural magnetic resonance imaging, J. Alzheimers Dis. 41 (2014) 685–708.
[42] N. Tzourio-Mazoyer, B. Landeau, D. Papathanassiou, F. Crivello, O. Etard, N. Delcroix, B. Mazoyer, M. Joliot, Automated anatomical labeling of activations in SPM using a macroscopic anatomical parcellation of the MNI MRI single-subject brain, Neuroimage 15 (2002) 273–289.
[43] N.U.F. Dosenbach, B. Nardos, A.L. Cohen, D.A. Fair, J.D. Power, J.A. Church, S.M. Nelson, G.S. Wig, A.C. Vogel, C.N. Lessov-Schlaggar, K.A. Barnes, J.W. Dubis, E. Feczko, R.S. Coalson, J.R. Pruett, D.M. Barch, S.E. Petersen, B.L. Schlaggar, Prediction of individual brain maturity using fMRI, Science 329 (2010) 1358–1361.
[44] R.S. Desikan, F. Segonne, B. Fischl, B.T. Quinn, B.C. Dickerson, D. Blacker, R.L. Buckner, A.M. Dale, R.P. Maguire, B.T. Hyman, M.S. Albert, R.J. Killiany, An automated labeling system for subdividing the human cerebral cortex on MRI scans into gyral based regions of interest, Neuroimage 31 (2006) 968–980.
[45] B. Fischl, A. van der Kouwe, C. Destrieux, E. Halgren, F. Segonne, D.H. Salat, E. Busa, L.J. Seidman, J. Goldstein, D. Kennedy, V. Caviness, N. Makris, B. Rosen, A.M. Dale, Automatically parcellating the human cerebral cortex, Cerebr. Cortex 14 (2004) 11–22.
[46] C.R. Jack Jr., M.A. Bernstein, N.C. Fox, P. Thompson, G. Alexander, D. Harvey, B. Borowski, P.J. Britson, L.W. J, C. Ward, A.M. Dale, J.P. Felmlee, J.L. Gunter, D.L. Hill, R. Killiany, N. Schuff, S. Fox-Bosetti, C. Lin, C. Studholme, C.S. DeCarli, G. Krueger, H.A. Ward, G.J. Metzger, K.T. Scott, R. Mallozzi, D. Blezek, J. Levy, J.P. Debbins, A.S. Fleisher, M. Albert, R. Green, G. Bartzokis, G. Glover, J. Mugler, M.W. Weiner, The Alzheimer's disease neuroimaging initiative (ADNI): MRI methods, J. Magn. Reson. Imag. 27 (2008) 685–691.
[47] Y. Chao-Gan, Z. Yu-Feng, DPARSF: a MATLAB toolbox for "pipeline" data analysis of resting-state fMRI, Front. Syst. Neurosci. 4 (2010) 13.
[48] M.D. Greicius, B. Krasnow, A.L. Reiss, V. Menon, Functional connectivity in the resting brain: a network analysis of the default mode hypothesis, Proc. Natl. Acad. Sci. U. S. A. 100 (2003) 253–258.
[49] F. Segonne, A.M. Dale, E. Busa, M. Glessner, D. Salat, H.K. Hahn, B. Fischl, A hybrid approach to the skull stripping problem in MRI, Neuroimage 22 (2004) 1060–1075.
[50] B. Fischl, D.H. Salat, E. Busa, M. Albert, M. Dieterich, C. Haselgrove, A. van der Kouwe, R. Killiany, D. Kennedy, S. Klaveness, A. Montillo, N. Makris, B. Rosen, A.M. Dale, Whole brain segmentation: automated labeling of neuroanatomical structures in the human brain, Neuron 33 (2002) 341–355.
[51] B. Fischl, D.H. Salat, A.J. van der Kouwe, N. Makris, F. Segonne, B.T. Quinn, A.M. Dale, Sequence-independent segmentation of magnetic resonance images, Neuroimage 23 (Suppl 1) (2004) S69–S84.
[52] B. Fischl, A. Liu, A.M. Dale, Automated manifold surgery: constructing geometrically accurate and topologically correct models of the human cerebral cortex, IEEE Trans. Med. Imag. 20 (2001) 70–80.
[53] A.M. Dale, B. Fischl, M.I. Sereno, Cortical surface-based analysis. I. Segmentation and surface reconstruction, Neuroimage 9 (1999) 179–194.
[54] B. Fischl, A.M. Dale, Measuring the thickness of the human cerebral cortex from magnetic resonance images, Proc. Natl. Acad. Sci. U. S. A. 97 (2000) 11050–11055.
[55] B. Fischl, M.I. Sereno, A.M. Dale, Cortical surface-based analysis. II: inflation, flattening, and a surface-based coordinate system, Neuroimage 9 (1999) 195–207.
[56] C. Destrieux, B. Fischl, A. Dale, E. Halgren, Automatic parcellation of human cortical gyri and sulci using standard anatomical nomenclature, Neuroimage 53 (2010) 1–15.
[57] D.S. Bassett, E.T. Bullmore, A. Meyer-Lindenberg, J.A. Apud, D.R. Weinberger, R. Coppola, Cognitive fitness of cost-efficient brain functional networks, Proc. Natl.

Acad. Sci. U.S.A. 106 (2009) 11747–11752.
[58] S.I. Dimitriadis, N.A. Laskaris, V. Tsirka, M. Vourkas, S. Micheloyannis, S. Fotopoulos, Tracking brain dynamics via time-dependent network analysis, J. Neurosci. Meth. 193 (2010) 145–155.
[59] J.D. Kruschwitz, D. List, L. Waller, M. Rubinov, H. Walter, GraphVar: a user-friendly toolbox for comprehensive graph analyses of functional brain connectivity, J. Neurosci. Meth. 245 (2015) 107–115.
[60] E. Estrada, J.A. Rodriguez-Velazquez, Subgraph centrality in complex networks, Phys. Rev. 71 (2005) 056103.
[61] M. Rubinov, O. Sporns, Complex network measures of brain connectivity: uses and interpretations, Neuroimage 52 (2010) 1059–1069.
[62] O. Voevodskaya, A. Simmons, R. Nordenskjold, J. Kullberg, H. Ahlstrom, L. Lind, L.O. Wahlund, E.M. Larsson, E. Westman, I. Alzheimer's Disease Neuroimaging, The effects of intracranial volume adjustment approaches on multiple regional MRI volumes in healthy aging and Alzheimer's disease, Front. Aging Neurosci. 6 (2014) 264.
[63] R. Jenkins, N.C. Fox, A.M. Rossor, R.J. Harvey, M.N. Rossor, Intracranial volume and Alzheimer disease: evidence against the cerebral reserve hypothesis, Arch. Neurol. 57 (2000) 220–224.
[64] J. Yang, Zexuan Zhu, He Shan, Zhen Ji, Minimal-redundancy-maximal-relevance feature selection using different relevance measures for omics data classification, Computational Intelligence in Bioinformatics and Computational Biology (CIBCB) IEEE, Apr 16 2013, pp. 246–251.
[65] Y. Fan, N. Batmanghelich, C.M. Clark, C. Davatzikos, I. Alzheimer's Disease Neuroimaging, Spatial patterns of brain atrophy in MCI patients, identified via high-dimensional pattern classification, predict subsequent cognitive decline, Neuroimage 39 (2008) 1731–1743.
[66] A.J. Smola, B. Schölkopf, A tutorial on support vector regression, Stat. Comput. 14 (2004) 199–222.
[67] A. Zalesky, A. Fornito, E.T. Bullmore, Network-based statistic: identifying differences in brain networks, Neuroimage 53 (2010) 1197–1207.
[68] B.C. Dickerson, R.A. Sperling, Functional abnormalities of the medial temporal lobe memory system in mild cognitive impairment and Alzheimer's disease: insights from functional MRI studies, Neuropsychologia 46 (2008) 1624–1635.
[69] P. Coleman, H. Federoff, R. Kurlan, A focus on the synapse for neuroprotection in Alzheimer disease and other dementias, Neurology 63 (2004) 1155–1162.
[70] D.J. Selkoe, Alzheimer's disease is a synaptic failure, Science 298 (2002) 789–791.
[71] E. Moradi, A. Pepe, C. Gaser, H. Huttunen, J. Tohka, I. Alzheimer's Disease Neuroimaging, Machine learning framework for early MRI-based Alzheimer's conversion prediction in MCI subjects, Neuroimage 104 (2015) 398–412.
[72] E. Westman, A. Simmons, J.S. Muehlboeck, P. Mecocci, B. Vellas, M. Tsolaki, I. Kloszewska, H. Soininen, M.W. Weiner, S. Lovestone, C. Spenger, L.O. Wahlund, c. AddNeuroMed, I. Alzheimer's Disease Neuroimaging, AddNeuroMed and ADNI: similar patterns of Alzheimer's atrophy and automated MRI classification accuracy in Europe and North America, Neuroimage 58 (2011) 818–828.
[73] G. Chen, B.D. Ward, G. Chen, S.J. Li, Decreased effective connectivity from cortices to the right parahippocampal gyrus in Alzheimer's disease subjects, Brain Connect. 4 (2014) 702–708.
[74] C. Xie, F. Bai, H. Yu, Y. Shi, Y. Yuan, G. Chen, W. Li, G. Chen, Z. Zhang, S.J. Li, Abnormal insula functional network is associated with episodic memory decline in amnestic mild cognitive impairment, Neuroimage 63 (2012) 320–327.
[75] M. Daianu, E.L. Dennis, N. Jahanshad, T.M. Nir, A.W. Toga, C.R. Jack, M.W. Weiner, P.M. Thompson, Alzheimer's disease disrupts rich club organization in brain connectivity networks, Biomedical Imaging (ISBI), 2013 IEEE 10th International Symposium on, IEEE, 2013, pp. 266–269.
[76] G. Prasad, S.H. Joshi, T.M. Nir, A.W. Toga, P.M. Thompson, A.s.D.N. Initiative, Brain connectivity and novel network measures for Alzheimer's disease classification, Neurobiol. Aging 36 (2015) S121–S131.
[77] J. Hanggi, J. Streffer, L. Jancke, C. Hock, Volumes of lateral temporal and parietal structures distinguish between healthy aging, mild cognitive impairment, and Alzheimer's disease, J. Alzheim. Dis. 26 (2011) 719–734.
[78] S.L. Risacher, A.J. Saykin, J.D. West, L. Shen, H.A. Firpi, B.C. McDonald, I. Alzheimer's Disease Neuroimaging, Baseline MRI predictors of conversion from MCI to probable AD in the ADNI cohort, Curr. Alzheimer Res. 6 (2009) 347–361.
[79] L. Wang, F.C. Goldstein, E. Veledar, A.I. Levey, J.J. Lah, C.C. Meltzer, C.A. Holder, H. Mao, Alterations in cortical thickness and white matter integrity in mild cognitive impairment measured by whole-brain cortical thickness mapping and diffusion tensor imaging, AJNR Am. J. Neuroradiol. 30 (2009) 893–899.
[80] E. Westman, C. Aguilar, J.S. Muehlboeck, A. Simmons, Regional magnetic resonance imaging measures for multivariate analysis in Alzheimer's disease and mild cognitive impairment, Brain Topogr. 26 (2013) 9–23.
[81] A. Abu-Akel, S. Shamay-Tsoory, Neuroanatomical and neurochemical bases of theory of mind, Neuropsychologia 49 (2011) 2971–2984.
[82] D.J. Bonthius, A. Solodkin, G.W. Van Hoesen, Pathology of the insular cortex in Alzheimer disease depends on cortical architecture, J. Neuropathol. Exp. Neurol. 64 (2005) 910–922.
[83] W.W. Seeley, Anterior insula degeneration in frontotemporal dementia, Brain Struct. Funct. 214 (2010) 465–475.
[84] W.W. Seeley, D.A. Carlin, J.M. Allman, M.N. Macedo, C. Bush, B.L. Miller, S.J. DeArmond, Early frontotemporal dementia targets neurons unique to apes and humans, Ann. Neurol. 60 (2006) 660–667.
[85] S.E. Arnold, B.T. Hyman, J. Flory, A.R. Damasio, G.W. Van Hoesen, The topographical and neuroanatomical distribution of neurofibrillary tangles and neuritic plaques in the cerebral cortex of patients with Alzheimer's disease, Cerebr. Cortex 1 (1991) 103–116.
[86] C.R. McDonald, L.K. McEvoy, L. Gharapetian, C. Fennema-Notestine, D.J. Hagler Jr., D. Holland, A. Koyama, J.B. Brewer, A.M. Dale, I. Alzheimer's Disease Neuroimaging, Regional rates of neocortical atrophy from normal aging to early Alzheimer disease, Neurology 73 (2009) 457–465.
[87] E. Salmon, P. Ruby, D. Perani, E. Kalbe, S. Laureys, S. Adam, F. Collette, Two aspects of impaired consciousness in Alzheimer's disease, Prog. Brain Res. 150 (2005) 287–298.